SIMULATION NUMÉRIQUE D'UN ÉCOULEMENT DIPHASIQUE COMPRESSIBLE AVEC LE SCHÉMA HLLC AVEC LE SOLVEUR NSMB

NUMERICAL SIMULATION OF COMPRESSIBLE TWO-PHASE FLOW WITH HLLC SCHEME IN NSMB SOLVER

A.K. GUN[(1)], E. GONCALVES[(2)], Y. HOARAU[(3)]

anil-kemal.gun@etu.unistra.fr ; eric.goncalves@ensma.fr ; hoarau@unistra.fr

[(1)]University of Strasbourg, ICUBE laboratory, UMR 7357 CNRS, 67000 Strasbourg, France
[(2)]ISAE-ENSMA, Institut Pprime, UPR 3346 CNRS, 86961 Futuroscope Chasseneuil, France
[(3)]University of Strasbourg, ICUBE laboratory, UMR 7357 CNRS, 67000 Strasbourg, France

Résumé

Cette étude examine la solution numérique de problèmes diphasiques en utilisant le modèle réduit de Kapila, c'est-à-dire le modèle à quatre équations. Ce modèle a été testé sur différents cas tests en utilisant le schéma numérique HLLC et ses extensions. Les résultats révèlent que la plupart des stratégies de reconstruction produisent des résultats qui sont en bon accord avec la solution de référence. Cependant, certaines divergences ont également été trouvées. Ce travail est préliminaire pour valider les capacités du solveur NSMB pour les écoulements diphasiques et est destiné à ouvrir la voie d'autres modèles d'écoulement diphasique dont l'ajout au solveur est prévu.

Summary

This study examines the numerical solution of two-phase problems using the reduced Kapila model, that is, the four-equation model. This model was tested on different test cases using the HLLC numerical scheme and its extensions. The results reveal that most reconstruction strategies produce results that are in good agreement with the reference solutions. However, certain discrepancies have also been found. This work is preliminary to validate the capabilities of the NSMB solver for two-phase flows and is intended to pave the way for other two-phase flow models planned to be added to the solver.

I – Introduction

For different applications dealing with two-phase flows such as nuclear safety, cavitation, turbo-machinery, etc., it is necessary to develop a compressible numerical tool to properly capture the large variety of thermodynamic properties, traveling waves, or stiff fronts. Although there has been an increase in compressible two-phase flow research recently, due to the hyperbolic nature of the system, the quality and complexity of the models and numerical simulations produced may vary. The averaged two-phase fluid flow model is the foundation of the most popular modeling methodology. Different strategies are used within this averaged model depending on the relevant physical assumptions made regarding the local mechanical and thermodynamical equilibrium as well as the phase slip condition. As a result, several models and systems of equations ranging in complexity from seven to just three equations have been developed. In this context, two-phase flow modeling has been implemented by the parallel Navier Stokes Multi Block (NSMB) solver. NSMB solver is a finite volume methods solver for the steady or unsteady Navier-Stokes equations in their compressible or incompressible versions on multi-block structured grids. In this study numerical solutions to two-phase problems will be examined utilizing the reduced Kapila model, a four-equation model, which consists of three conservation laws for mixture quantities and a void ratio for the transport equation. In particular, the focus was on HLLC (Harten-Lax-van Leer Contact) approximate Riemann solver and its extensions. These numerical methods were compared with test cases in the literature to validate the accuracy of the overall solver. In conclusion, implementation and validation studies on the NSMB solver will pave the way for other two-phase modeling types that are planned to be adapted to the solver to handle problems related to hypothetical loss-of-coolant accidents in nuclear reactors.

II – Governing equations

The 4-equation model [1] is a reduced version of the 5-equation Kapila model [4], assuming that the liquid is in the saturation state. The model consists in three conservation laws for mixture quantities and an additional equation for the void ratio. The phases are assumed strongly coupled and moving at the same velocity. In addition, the phases are assumed to be in thermal and mechanical equilibrium. Below can be found inviscid two-dimensional equations expressed in variables $w=(\rho,\rho\overrightarrow{V},\rho E,\alpha)$:

$$\frac{\partial \rho}{\partial t} + \mathrm{div}(\rho\overrightarrow{V}) = 0 \tag{2.1}$$

$$\frac{\partial(\rho\overrightarrow{V})}{\partial t} + \mathrm{div}(\rho\overrightarrow{V} \otimes \overrightarrow{V} + PId) = 0 \tag{2.2}$$

$$\frac{\partial(\rho E)}{\partial t} + \mathrm{div}(\rho\overrightarrow{V}H) = 0 \tag{2.3}$$

$$\frac{\partial \alpha}{\partial t} + \overrightarrow{V}.\mathrm{grad}(\alpha) = K\mathrm{div}(\overrightarrow{V}) \tag{2.4}$$

$$K = \frac{\rho_l c_l^2 - \rho_v c_v^2}{\frac{\rho_l c_l^2}{1-\alpha} + \frac{\rho_v c_v^2}{\alpha}} \tag{2.5}$$

where $\overrightarrow{V} = (u, v)$ denotes the centre of mass velocity, $E = e + V^2/2$ is the total energy of mixture and $H = h + V^2/2$ is the enthalpy of this mixture. The term K refers to the sound speed of pure phases c_k and it reflects the impacts of volume changes in each phase. An equation of state (EoS), which connects the pressure and temperature to the internal energy and density, is required to complete the system. For pure phases, convex stiffened gas EoS was used [5] :

$$P(\rho, e) = (\gamma - 1)\rho(e - q) - \gamma P_\infty \tag{2.6}$$

$$P(\rho, T) = \rho(\gamma - 1)C_v T - P_\infty \tag{2.7}$$

$$T(\rho, h) = \frac{h - q}{C_p} \tag{2.8}$$

where $\gamma = C_p/C_v$ is the heat capacity ratio, C_p and C_v are thermal capacities, q the energy of formation and P_∞ is a constant reference pressure. The speed of sound c is given by ;

$$c^2 = \gamma \frac{P + P_\infty}{\rho} = (\gamma - 1)C_p T \tag{2.9}$$

On the basis of the stiffened gas EOS, it is possible to derive a formula for the pressure and temperature for the two-phase mixture area using the thermal and mechanical equilibrium assumption [8]. These formulas, along with functions for the void fraction α and the mass fraction of gas Y, are available in all possible fluid states :

$$P(\rho, e, \alpha, Y) = (\gamma(\alpha) - 1)\rho(e - q(Y)) - \gamma(\alpha)P_\infty(\alpha) \tag{2.10}$$

$$\frac{1}{\gamma(\alpha) - 1} = \frac{\alpha}{\gamma_v - 1} + \frac{1 - \alpha}{\gamma_l - 1} \tag{2.11}$$

$$q(Y) = Y q_v + (1 - Y)q_l \tag{2.12}$$

$$P_\infty(\alpha) = \frac{\gamma(\alpha) - 1}{\gamma(\alpha)} \left[\alpha \frac{\gamma_v}{\gamma_v - 1} P_\infty^v + (1 - \alpha)\frac{\gamma_l}{\gamma_l - 1} P_\infty^l \right] \tag{2.13}$$

$$T(\rho, h, Y) = \frac{h - q(Y)}{C_p(Y)} \tag{2.14}$$

$$C_p(Y) = Y C_{p_v} + (1 - Y)C_{p_l} \tag{2.15}$$

Acoustic waves propagate at the Wallis speed of sound in the absence of mass transfer. This speed is denoted by :

$$\frac{1}{\rho c_{wallis}^2} = \frac{\alpha}{\rho_v c_v^2} + \frac{1 - \alpha}{\rho_l c_l^2} \tag{2.16}$$

3

The mass transfer term is activated when the local pressure P is smaller than the vapour pressure $P_{vap}(T)$ which is calculated as :

$$P_{vap}(T) = P_{vap}(T_{ref}) + \frac{dP}{dT}(T - Tref) \tag{2.17}$$

The void ratio equation expression changes when mass transfer between phases takes place, and becoming :

$$\frac{\partial \alpha}{\partial t} + \text{div}(\alpha \overrightarrow{V}) = (K + \alpha)\text{div}(\overrightarrow{V}) + \left(\frac{\frac{c_v^2}{\alpha} + \frac{c_l^2}{1-\alpha}}{\frac{\rho_l c_l^2}{1-\alpha} + \frac{\rho_v c_v^2}{\alpha}} \right) \dot{m} \tag{2.18}$$

It is possible to create a family of models in which $\dot{m}$ is expressed as by assuming that the mass transfer is proportional to the divergence of the velocity [2] :

$$\dot{m} = \frac{\rho_l \rho_v}{\rho_l - \rho_v} \left(1 - \frac{c^2}{c_{wallis}^2} \right) \text{div}(\overrightarrow{V}) \tag{2.19}$$

The enthalpy of each phase can be used to describe the speed of sound in the mixture [3] :

$$\rho c^2 = (\gamma(\alpha) - 1) \left[\frac{\rho_v \rho_l}{(\rho_l - \rho_v)} (h_v - h_l) \right] \tag{2.20}$$

III – Numerical method

The four-equations model can be represented as a matrix in one-dimensional space as :
$$\frac{\partial w}{\partial t} + \frac{\partial F(w)}{\partial x} = S(w) \tag{2.21}$$
where $S(w)$ source term, F convective flux and $w = (\rho, \rho u, \rho E, \alpha)$ is the vector of conserved variables. Using the finite volume technique, the computational domain can be divided into regular meshes, if this is done for the spatial domain and the temporal domain, the above equation can be reformulated as follows :

$$\Delta x \frac{w_i^{n+1} - w_i^n}{\Delta t} + F_{i+1/2}^n - F_{i-1/2}^n = S_i^n \Delta x \tag{2.22}$$

where i and n stand for discretization in space and time, respectively. This numerical flux can be calculated using a Riemann problem solution or any other numerical method. Although the main problem here arises from the non-conversavite form of the conservation equations and the existence of the source term, different approaches can be found in the literature to solve such problems. In this study, numerical simulations are performed using an explicit time integration and the convective flux through the cell interface is calculated with an HLLC scheme [10]. The HLLC approach takes into account two averaged intermediate states, w_L^* and w_R^*, separated by the contact wave speed S_M. At a cell interface, the numerical flow $F_{i+1/2}$ can be represented as :

$$F_{i+1/2} = \begin{cases} F(w_L), & \text{if} \quad S_L > 0 \\ F(w_L^*), & \text{if} \quad S_L \leq 0 < S_M \\ F(w_R^*), & \text{if} \quad S_M \leq 0 \leq S_R \\ F(w_R), & \text{if} \quad S_R < 0 \end{cases} \tag{2.23}$$

The speeds of the smallest and largest waves at the cell interface are referred to as S_L and S_R, respectively. $F(w_k^*)$, P^*, S_M are defined as follows :

$$w_K^* = \begin{pmatrix} \rho_K^* \\ (\rho u)_K^* \\ (\rho E)_K^* \\ \alpha_K^* \end{pmatrix} \tag{2.24}$$

$$w_K^* = \frac{1}{S_K - S_M} \begin{pmatrix} \rho_K(S_K - u_K) \\ (\rho u)_K(S_K - u_K) + P^* - P_K \\ (\rho E)_K(S_K - u_K) + P^* S_M - P_K u_K \\ \alpha_K(S_K - u_K) \end{pmatrix} \tag{2.25}$$

$$F(w_K^*) = \begin{pmatrix} \rho_k^* S_M \\ (\rho u)_K^* S_M + P^* \\ (\rho E)_K^* S_M + P^* S_M \\ \alpha_K^* S_M \end{pmatrix} \tag{2.26}$$

$$P^* = P_L + \rho_L(u_L - S_L)(u_L - S_M) = P_R + \rho_R(u_R - S_R)(u_R - S_M) \tag{2.27}$$

$$S_M = \frac{P_R - P_L + \rho_L u_L(S_L - u_L) - \rho_R u_R(S_R - u_R)}{\rho_L(S_L - u_L) - \rho_R(S_R - u_R)} \tag{2.28}$$

We also need the wave speeds S_L and S_R to fully determine the numerical fluxes. Although there are different approaches related to this in the literature, simple wave speed estimation is used :

$$S_L = Min(u_L - c_L, u_R - c_R) \qquad S_R = Max(u_L + c_L, u_R + c_R)$$

Over the past decades, a tremendous amount of research has been done to develop high-resolution methods for hyperbolic conservation laws, as a result, there are different methods that can be found to achieve high-order accuracy in the literature. The earliest significant contribution to this direction is the MUSCL (*Monotone Upstream-centred Scheme for Conservation Laws*) scheme by van Leer. Since van Leer's work, the MUSCL scheme has been studied by many experts and is widely used for simulations of scientific and engineering problems, and this method has also been applied in this study. The concept is to use reconstructed states to replace the piecewise constant approximation of Godunov's method, which is formed from cell-averaged states from the previous time step. In this way, slope limited, reconstructed left and right states are obtained for each cell and utilized to calculate fluxes at cell boundaries. As known, high order schemes produce spurious oscillations. Therefore, in this study, van Leer slope limiter is applied to avoid the spurious oscillations.

IV – Results

Case 1

This test case is proposed in [9]. A one-meter-long shock tube with two chambers and chambers separated at x = 0.6 m. The initial volume fraction of spinel is 0.4046 everywhere. The pressure in the left chamber is 10^{10} Pa while the right chamber is at atmospheric pressure. The fluids are initially at rest and are governed by the stiffened gas EOS. The parameters are :

$$\begin{pmatrix} \gamma \\ P_\infty \\ \rho \end{pmatrix}_{Epoxy} = \begin{pmatrix} 2.43 \\ 5.3 \times 10^9 \text{ Pa} \\ 1185 \text{ kg/m}^3 \end{pmatrix} \text{ and } \begin{pmatrix} \gamma \\ P_\infty \\ \rho \end{pmatrix}_{Spinel} = \begin{pmatrix} 1.62 \\ 141 \times 10^9 \text{ Pa} \\ 3622 \text{ kg/m}^3 \end{pmatrix} \quad (3.1)$$

Results are displayed in 80 µs, calculations are made with a mesh of 6000 cells and the results are compared to the exact solution [7]. While void ratio and mixture density profiles are shown in Figure 1, mixture pressure and velocity are presented in Figure 2. HLLC 2 and HLLC 3 refer to the second and third-order extensions. As can be seen, the results are quite similar except for some deviations in HLLC third-order scheme.
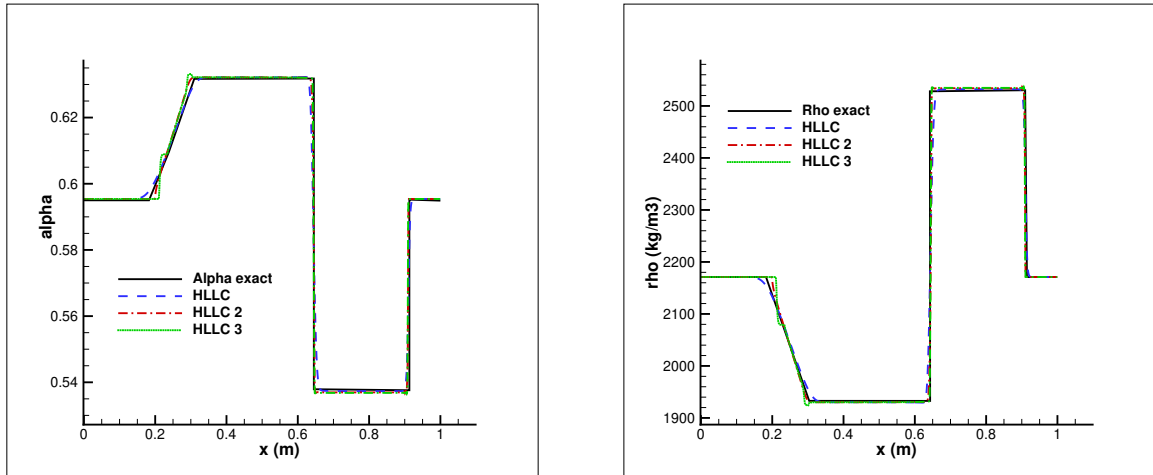
FIGURE 1 – Void ratio and mixture density profiles along the tube, case 1, t=80 µs.

Case 2

This test case is proposed in [8]. A one meter long shock tube where left chamber filled with liquid dodecane at 10^8 Pa and with density 500 kg/m^3, while right chamber filled with vapor dodecane at atmospheric pressure and with density 2 kg/m^3. The initial discontinuity is located at x = 0.75 m and each chamber contains a weak volume fraction (10^{-8}) of the other fluid. The fluids are initially at rest and are governed by the stiffened gas EoS. The parameters are :

$$\begin{pmatrix} P_\infty \\ C_p \\ C_v \\ \gamma \\ q \end{pmatrix}_{Liquid} = \begin{pmatrix} 4 \times 10^8 \text{ Pa} \\ 2534 \text{ J kg}^{-1} \text{ K}^{-1} \\ 1077 \text{ J kg}^{-1} \text{ K}^{-1} \\ 2.35 \\ -755 \times 10^3 \text{ J kg}^{-1} \end{pmatrix} \text{ and } \begin{pmatrix} P_\infty \\ C_p \\ C_v \\ \gamma \\ q \end{pmatrix}_{Vapor} = \begin{pmatrix} 0 \\ 2005 \text{ J kg}^{-1} \text{ K}^{-1} \\ 1956 \text{ J kg}^{-1} \text{ K}^{-1} \\ 1.025 \\ -237 \times 10^3 \text{ J kg}^{-1} \end{pmatrix} \quad (3.2)$$
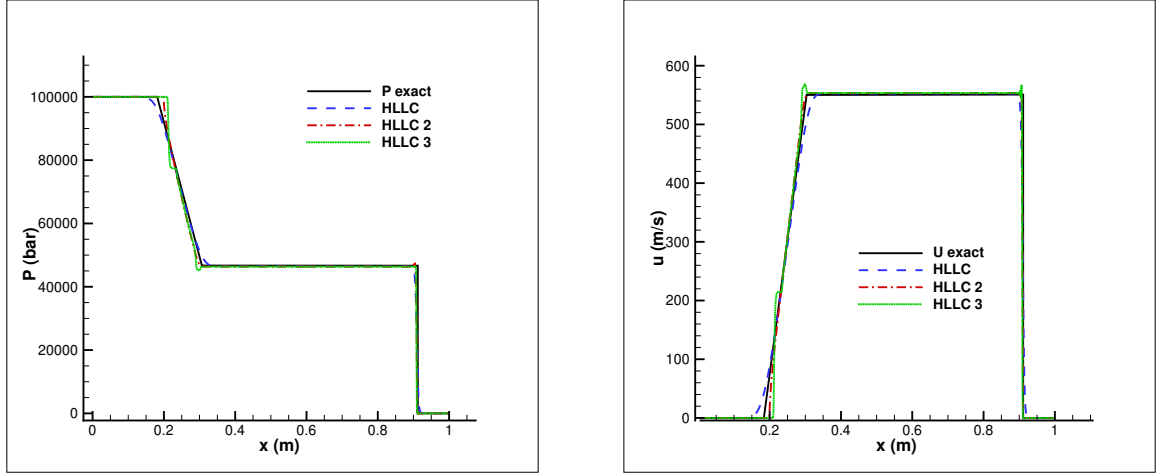
FIGURE 2 – Mixture pressure and velocity profiles along the tube, case 1, t=80 µs.

Results are displayed in 473 µs, calculations are made with a mesh of 6000 cells and the results are compared to the exact solution. While void ratio and mixture density profiles are shown in Figure 3, mixture pressure and velocity are presented in Figure 4. While the void ratio and density results were very close to the reference result, some inconsistency was observed in the velocity results and there was a significant fluctuation in the pressure results.
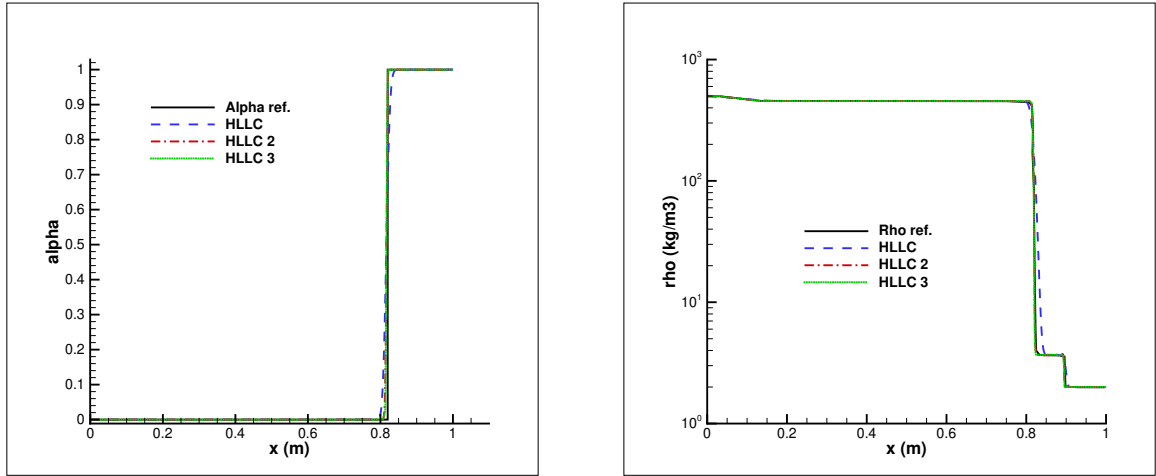
FIGURE 3 – Void ratio and mixture density profiles along the tube, case 2, t=473 µs.

Case 3

This test case is proposed in [9]. A one-meter-long shock tube with two chambers. The left chamber contains high-pressure fluid (10^9 Pa) while the right chamber contains low-pressure fluid (10^5 Pa). Chambers are separated by an interface at the location x = 0.75 m. In the left chamber, the water volume fraction is set to $\alpha_{water} = 1 - \epsilon$ and in the right chamber its value is $\alpha_{water} = \epsilon$, with $\epsilon = 10^{-6}$. The fluids are governed by the stiffened gas EoS;

$$\begin{pmatrix} \gamma \\ P_\infty \\ \rho \end{pmatrix}_{Liq} = \begin{pmatrix} 4.4 \\ 6 \times 10^8 \text{ Pa} \\ 1000 \text{ kg/m}^3 \end{pmatrix} \text{ and } \begin{pmatrix} \gamma \\ P_\infty \\ \rho \end{pmatrix}_{Gas} = \begin{pmatrix} 1.4 \\ 0 \text{ Pa} \\ 1 \text{ kg/m}^3 \end{pmatrix} \tag{3.3}$$

7
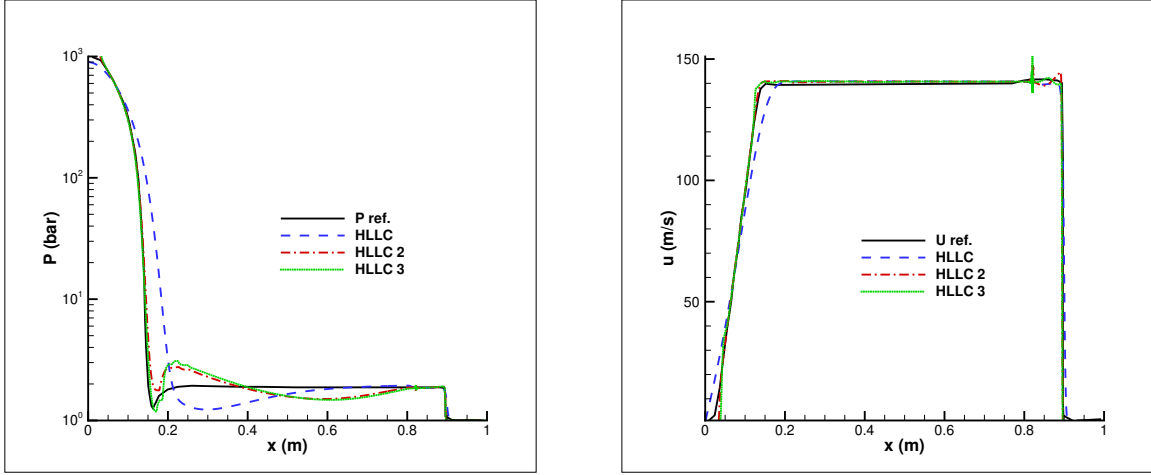
FIGURE 4 – Mixture pressure and velocity profiles along the tube, case 2, t=473 µs.

Results are displayed in 240 µs, calculations are made with a mesh of 4000 cells and the results are compared to the exact solution of the Euler equations. While void ratio and mixture density profiles are shown in Figure 5, mixture pressure and velocity are presented in Figure 6. As can be seen, the results are similar except for the post-shock values of the velocity. Also, some discrepancy is observed in the HLLC third-order scheme.
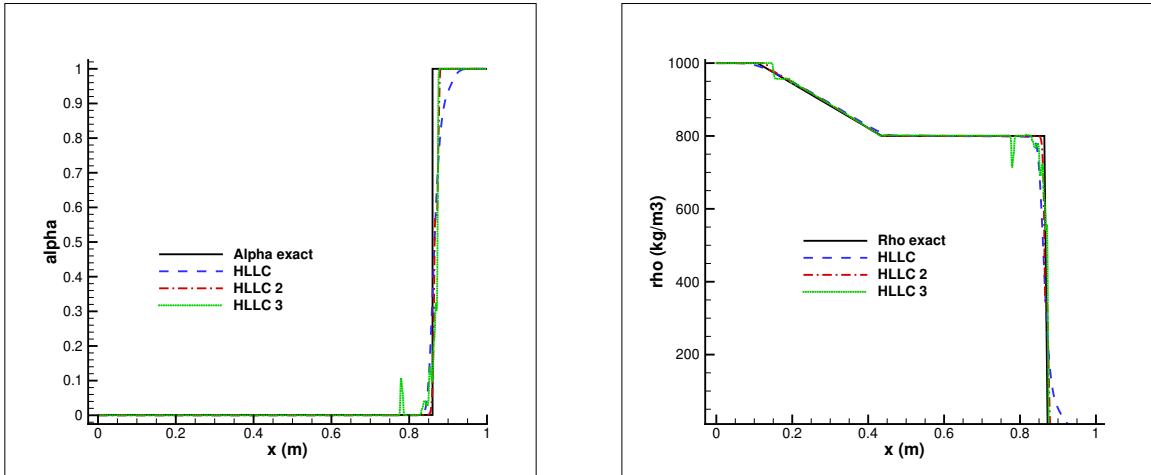
FIGURE 5 – Void ratio and mixture density profiles along the tube, case 3, t=240 µs.

Case 4

This test case is proposed in [6]. A one-meter-long shock tube with two chambers. The left chamber contains high pressure fluids (10^9 Pa) while the right chamber contains low pressure fluids (10^5 Pa). For x < 0.7 m the liquid volume fraction is 0.8, while it is 0.2 otherwise. The fluids are initially at rest and are governed by the stiffened gas EoS, and these characteristics are the same as in the above test case (3.3). Results are displayed at a time of 0.2 ms, the computations were done with a mesh of 6000 cells and the results are compared to reference 5-equation reduced model solution [6]. While void ratio and mixture density profiles are shown in Figure 7, mixture pressure and velocity are presented in Figure 8. In high-order schemes, deviations are observed in the post-shock values of velocity and density compared to the reference result. Also, in high orders, the head of the rarefaction wave location deviates from the reference result.

8
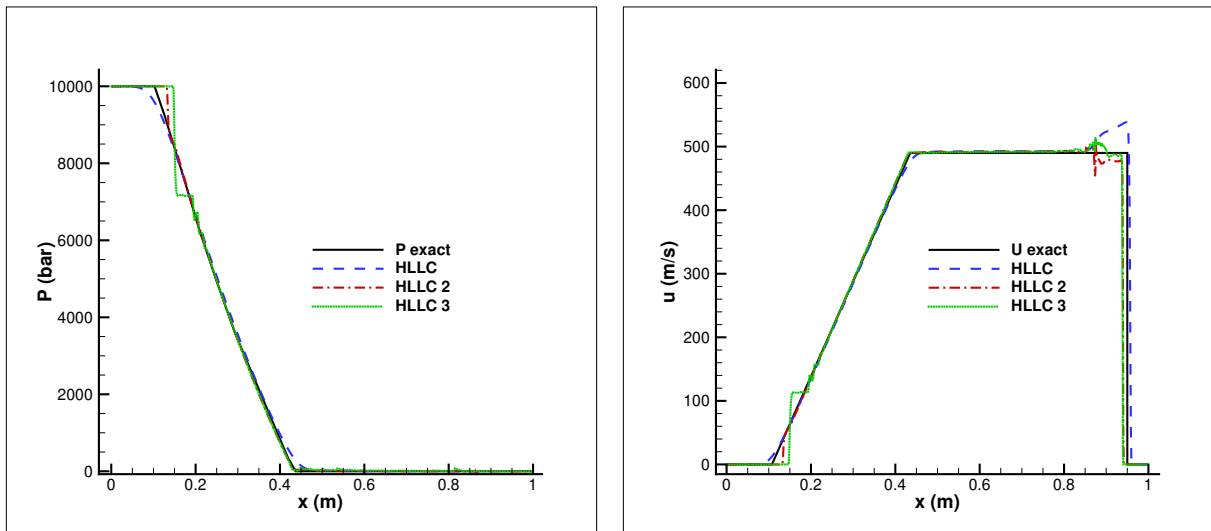
FIGURE 6 – Mixture pressure and velocity profiles along the tube, case 3, t=240 µs.
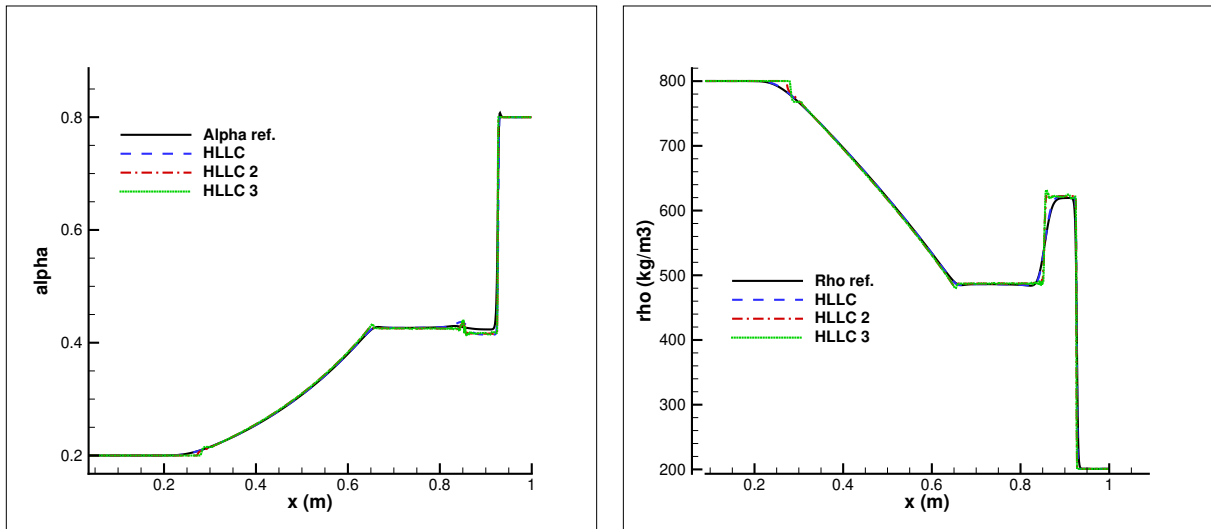
FIGURE 7 – Void ratio and mixture density profiles along the tube, case 4, t=0.2 ms.
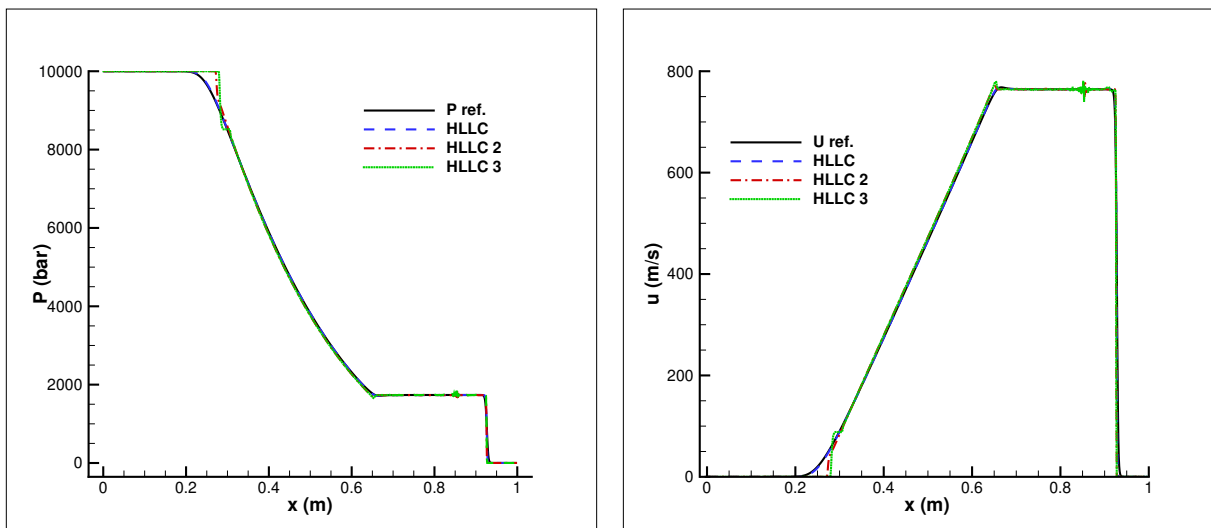
FIGURE 8 – Mixture pressure and velocity profiles along the tube, case 4, t=0.2 ms.

Case 5

With an initial velocity discontinuity situated in the middle of the tube, a problem involving a double rarefaction tube is taken into consideration, and proposed in [11]. A one-meter long tube filled with liquid water at atmospheric pressure and with density 1150 kg/m^3 will be used for this test. A weak volume fraction of vapor is 0.01 initially added to the liquid. The left velocity is -2 m/s while right velocity 2 m/s, and fluid are governed by the stiffened gas EoS;

$$
\begin{pmatrix} \gamma \\ P_\infty \\ q \\ \rho \\ C_p \end{pmatrix}_{Liq} = \begin{pmatrix} 2.35 \\ 10^9 \text{ Pa} \\ -0.1167 \times 10^7 \text{ J kg}^{-1} \\ 1150 \text{ kg/m}^3 \\ 4267 \text{ J kg}^{-1} \text{ K}^{-1} \end{pmatrix} \text{ and } \begin{pmatrix} \gamma \\ P_\infty \\ q \\ \rho \\ C_p \end{pmatrix}_{Gas} = \begin{pmatrix} 1.43 \\ 0 \text{ Pa} \\ 0.2030 \times 10^7 \text{ J kg}^{-1} \\ 1 \text{ kg/m}^3 \\ 1487 \text{ J kg}^{-1} \text{ K}^{-1} \end{pmatrix} \quad (3.4)
$$

Result are displayed in 3.2 ms, calculations are made with a mesh of 6000 cells and the result are compared to the two-fluid solution. While void ratio and mixture density profiles are shown in Figure 9, mixture pressure and velocity are presented in Figure 10. The solution involves two expansion waves. Void ratio and mixture density profiles are inconsistent with reference results around the initial discontinuity region.
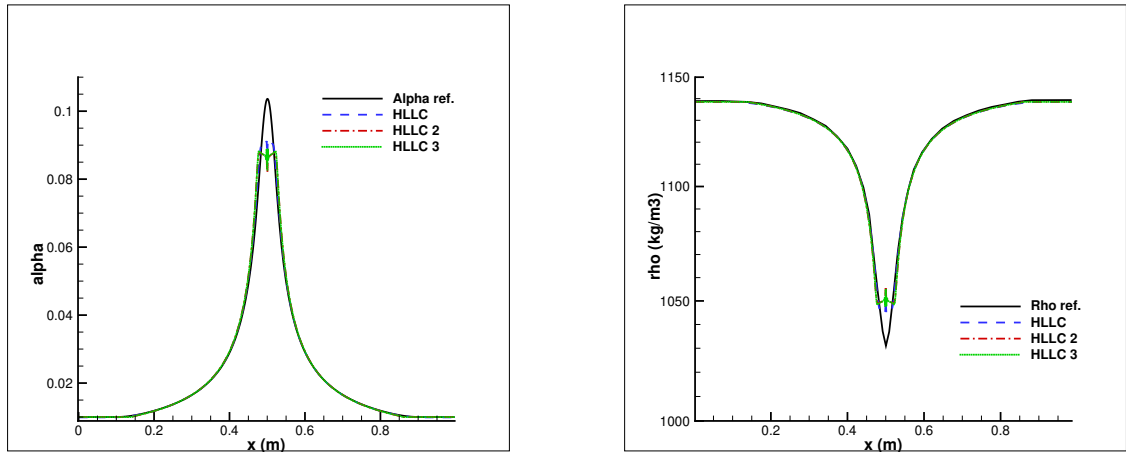
FIGURE 9 – Void ratio and mixture density profiles along the tube, case 5, t=3.2 ms.
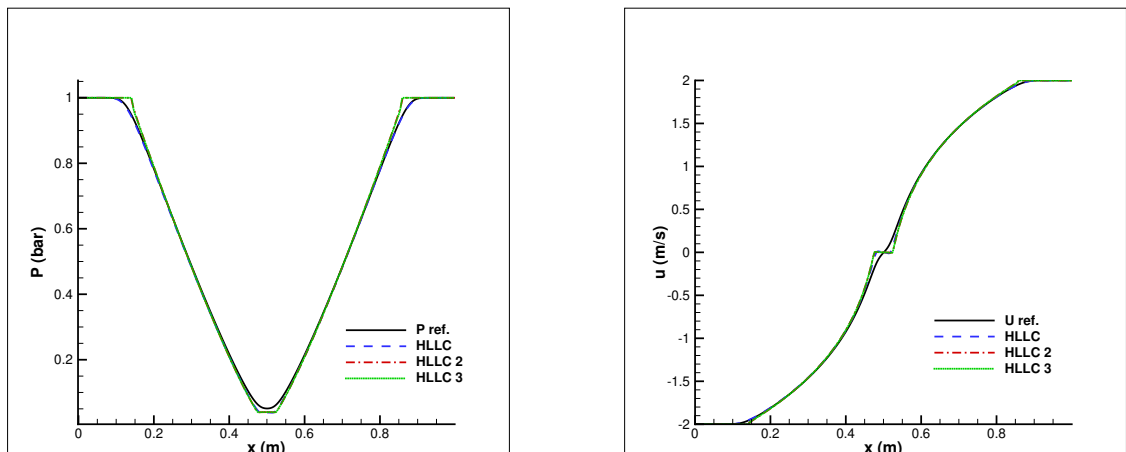
FIGURE 10 – Mixture pressure and velocity profiles along the tube, case 5, t=3.2 ms

Case 6

The final test case is obtained by adding the mass transfer term to the previous test case. As the liquid water expands until the saturation pressure is reached, evaporation begins to occur and a cavitation pocket is formed. Four expansion waves make up the solution with phase transition. The evaporation fronts are represented by the additional two expansion waves. The vapour pressure at the considered reference temperature is $P_{vap} = 51000$ Pa. 2044 Pa/K is used as the constant dP/dT estimated using a thermodynamic table.

Result are displayed in 3.2 ms, calculations are made with a mesh of 6000 cells and the result are compared to the two-fluid solution. While mixture pressure and velocity are shown in Figure 11, void ratio is presented in Figure 12. The void ratio is now close to 70% in the cavitation pocket as opposed to the prior scenario where values were around 10%. Although some deviations are observed in the pressure and velocity profile, the plateau of pressure at the vapor pressure value is well illustrated.
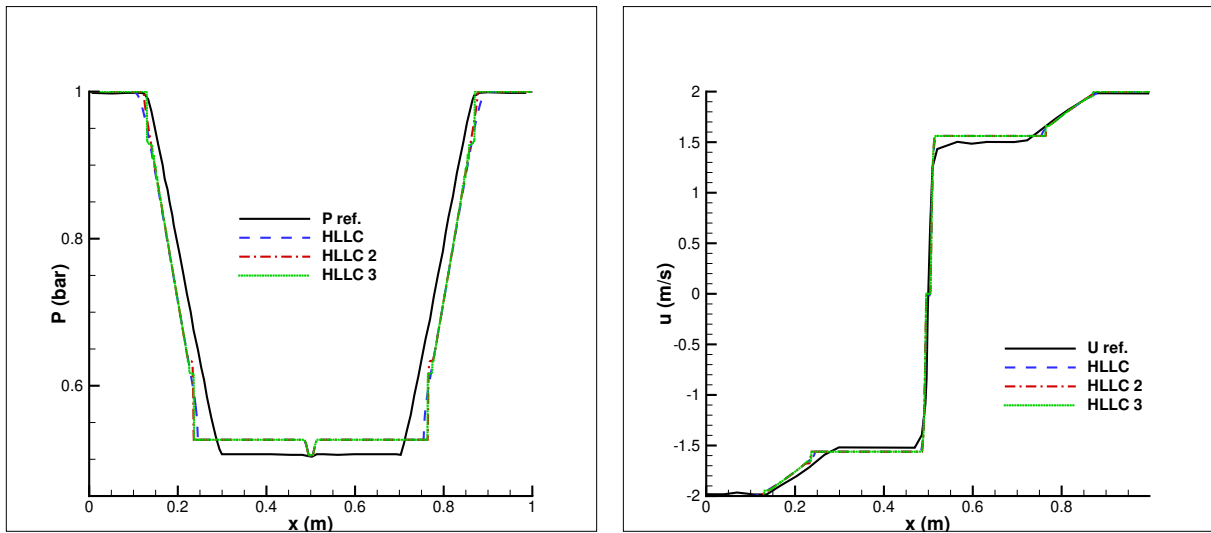
FIGURE 11 – Mixture pressure and velocity profiles along the tube, case 6, t=3.2 ms.
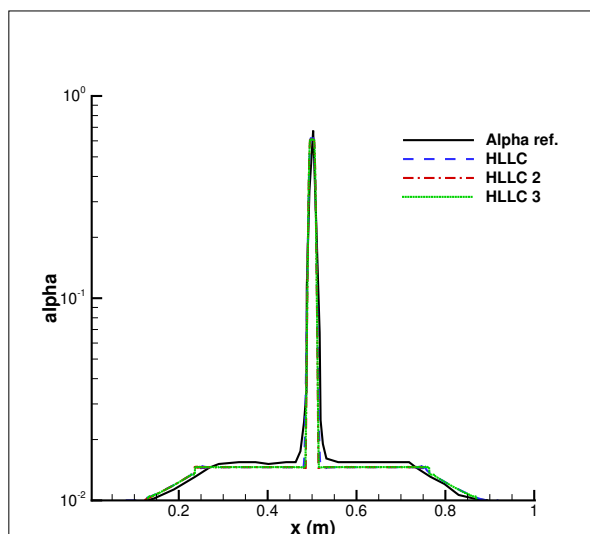
FIGURE 12 – Void ratio profile along the tube, case 6, t=3.2 ms.

V – Conclusion

Using the four-equation model, the numerical solution of two-phase problems is examined. This model was evaluated on several test cases using the HLLC numerical scheme and its expansions. When compared to the reference results, it has been found that some of the results obtained are satisfactory. However, discrepancy have been observed in some results. These results can be improved by using Hancock predictor corrector strategy. The ultimate goal of the studies is to simulate a hypothetical loss-of-coolant accident in nuclear power plants. However, a more complete methodology is desired to increase the accuracy of numerical simulations of nuclear safety accidents, and for this it is crucial to take into account thermal and chemical non-equilibrium. For this purpose, two new models are planned to be added to the NSMB solver, *homogeneous relaxation model* and *single velocity six-equation model.*

Références

[1] E. G. da Silva and D. Zeidan. Simulation of compressible two-phase flows using a void ratio transport equation. *Communications in Computational Physics*, 24(1) :167–203, 2018.

[2] E. Goncalvès. Numerical study of expansion tube problems : Toward the simulation of cavitation. *Computers & Fluids*, 72 :1–19, 2013.

[3] E. Goncalvès and B. Charrière. Modelling for isothermal cavitation with a four-equation model. *International Journal of Multiphase Flow*, 59 :54–72, 2014.

[4] A. Kapila, R. Menikoff, J. Bdzil, S. Son, and D. S. Stewart. Two-phase modeling of deflagration-to-detonation transition in granular materials : Reduced equations. *Physics of fluids*, 13(10) :3002–3024, 2001.

[5] O. Le Métayer, J. Massoni, R. Saurel, P. SMASH, et al. Elaborating equations of state of a liquid and its vapor for two-phase flow models ; elaboration des lois d'etat d'un liquide et de sa vapeur pour les modeles d'ecoulements diphasiques. *International journal of thermal sciences*, 43, 2004.

[6] A. Murrone and H. Guillard. A five equation reduced model for compressible two phase flow problems. *Journal of Computational Physics*, 202(2) :664–698, 2005.

[7] F. Petitpas, E. Franquet, R. Saurel, and O. Le Metayer. A relaxation-projection method for compressible flows. part ii : Artificial heat exchanges for multiphase shocks. *Journal of Computational Physics*, 225(2) :2214–2248, 2007.

[8] R. Saurel, F. Petitpas, and R. Abgrall. Modelling phase transition in metastable liquids : application to cavitating and flashing flows. *Journal of Fluid Mechanics*, 607 :313–350, 2008.

[9] R. Saurel, F. Petitpas, and R. A. Berry. Simple and efficient relaxation methods for interfaces separating compressible fluids, cavitating flows and shocks in multiphase mixtures. *journal of Computational Physics*, 228(5) :1678–1712, 2009.

[10] E. F. Toro. The equations of fluid dynamics. In *Riemann Solvers and Numerical Methods for Fluid Dynamics*, pages 1–40. Springer, 1999.

[11] A. Zein, M. Hantke, and G. Warnecke. Modeling phase transition for compressible two-phase flows applied to metastable liquids. *Journal of Computational Physics*, 229(8) :2964–2998, 2010.